

## Article

# Mechanism of Coal Burst Triggered by Disturbing Mining-Induced Stress: An Experimental Investigation

Jinzheng Bai <sup>1</sup>, Linming Dou <sup>1,2,\*</sup>, Xuwei Li <sup>1</sup>, Jinrong Cao <sup>1,3</sup>, Kangkang Wang <sup>1</sup>, Yanjiang Chai <sup>1,4</sup>  
and Jiliang Kan <sup>1</sup>

- <sup>1</sup> State Key Laboratory of Coal Resources and Safe Mining, School of Mines, China University of Mining and Technology, Xuzhou 221116, China
- <sup>2</sup> Jiangsu Engineering Laboratory of Mine Earthquake Monitoring and Prevention, School of Mines, China University of Mining and Technology, Xuzhou 221116, China
- <sup>3</sup> Geotechnical Institute, TU Bergakademie Freiberg, 09599 Freiberg, Germany
- <sup>4</sup> Zienkiewicz Centre for Computational Engineering, Faculty of Science and Engineering, Swansea University, Swansea SA1 8EP, UK
- \* Correspondence: dlm\_burst@126.com; Tel.: +86-1395-226-1972

**Abstract:** The true triaxial test can accurately simulate the dynamic and static load superposition environment of deep mining and then reproduce the spatial and temporal evolution process of coal-rock dynamic disasters. This study used a self-developed true triaxial coal-rock dynamic behavior test system to investigate the dynamic failure characteristics and mechanism of coal bursts under different mining-induced stress disturbances. The results show that the perturbation duration of the coal samples under quasi-static load decreases with the increase of the disturbance rate, and the perturbation stress level increases first and then decreases. The coal samples can accumulate higher strain energy and show progressive and dynamic failure. The perturbation duration and stress peak of the coal sample under the cycle load decreased with the increase of the cycle amplitude and frequency, and the coal sample first spalled off on the free surface. The damage then developed internally until the coal burst. The perturbation duration and stress peak of coal samples decrease with the increase of transient stress and the perturbation stress levels. The dynamic failure process of coal samples is straightforward, and the strength of coal burst is violent and is more difficult to predict. The conclusions obtained help to deepen the understanding of the triggering mechanism of coal bursts.

**Keywords:** coal burst; mining-induced stress; engineering disturbed; true triaxial test; dynamic failure characteristics



**Citation:** Bai, J.; Dou, L.; Li, X.; Cao, J.; Wang, K.; Chai, Y.; Kan, J. Mechanism of Coal Burst Triggered by Disturbing Mining-Induced Stress: An Experimental Investigation. *Appl. Sci.* **2022**, *12*, 10993. <https://doi.org/10.3390/app122110993>

Academic Editor: Arcady Dyskin

Received: 11 October 2022

Accepted: 27 October 2022

Published: 30 October 2022

**Publisher's Note:** MDPI stays neutral with regard to jurisdictional claims in published maps and institutional affiliations.



**Copyright:** © 2022 by the authors. Licensee MDPI, Basel, Switzerland. This article is an open access article distributed under the terms and conditions of the Creative Commons Attribution (CC BY) license (<https://creativecommons.org/licenses/by/4.0/>).

## 1. Introduction

Rock burst is one of the most severe dynamic disasters in underground mining. Coal and rock mass around a coal mining space is suddenly damaged and accompanied by an instant energy release [1,2]. Meanwhile, it tends to induce other dynamic disasters, such as coal and gas outbursts [3], gas explosions [4], water inrush [5], and earthquakes [6]. When this phenomenon occurs in a coal mine, it is typically referred to as a “coal burst” [7], which have happened in China, the United States, Poland, Australia, India, and South Africa, resulting in a large number of fatalities and economic losses [8–10]. Deep mining has become the normal state of coal resource acquisition. Therefore, it faces high ground stress, high temperatures, high osmotic pressure, and strong mining disturbance. The basic structure, mechanical properties, and engineering response characteristics of coal-rock mass have significant changes compared with the shallow part, leading to a more complex triggering mechanism of coal burst disaster.

The fundamental cause of deep coal-rock dynamic disasters is that manufactured mining activities destroy the initial equilibrium state. For a long time, mining stress

has been one of the essential topics in the field of accurate monitoring and prevention of coal bursts. The most intuitive manifestation of mining stress disturbance to coal-rock mass is the deformation and failure of coal around the mining space [11], such as roof subsidence, floor heave, surrounding rock shrinks, etc. Researchers have conducted extensive research on the physical and mechanical characteristics of coal-rock masses under different mining-induced stress disturbances, including deformation behavior [12], strength characteristics [13], mesoscopic structure [14], and permeability characteristics [15]. Zhang et al. [16] performed a series of laboratory tests on different damage degree rock mass, i.e., broken rock samples (caving zone), fracture coal samples (fracture zone and swelling deformation zone), and raw coal samples (original zone), to obtain permeability models for different damage zones surrounding the longwall face. Guo et al. proposed in situ experiments and three-dimensional numerical simulation and obtained coal's stress evolution and deformation characteristics under the mining stress path [17]. To study the effect of mining-induced stress on coal mining, Xue et al. experimentally evaluated the mechanical properties, acoustic emission characteristics, and energy evolution of coal masses [18]. Li et al. described the unloading mechanisms of brittle rock under different stress paths in two dimensions using the universal discrete element code PFC2D for numerical simulations [19]. Xue et al. analyzed the discontinuous solutions focused on quantitatively determining the radial and tangential stresses surrounding the roadways, the analytical values of the abutment pressure, and the horizontal stress ahead of the working face and their distributions [20].

The traditional theoretical design, analysis, and processing are widely used in deep rock engineering. The complex dynamic disturbance problems are often treated statically, which often causes stability and safety problems, and even leads to significant disasters. Mining disturbance is the unloading effect of mining activities on coal-rock mass in deep high-stress areas, manifested as a response of coal-rock mass from the original rock stress state to confining pressure unloading-axial loading state [21]. The static and dynamic responses of coal-rock mass under different stress disturbances are also different, affecting the instability and failure characteristics of coal-rock mass. However, the existing laboratory tests mainly focused on uniaxial, biaxial compression, or conventional triaxial loading. The research on the mechanical response of coal under different mining disturbance stress paths is still in its infancy. Therefore, to deeply investigate the triggering mechanism of coal burst in the complex dynamic and static load superposition environment of deep mining, it is necessary to consider the various mining-induced disturbances in deep coal mining.

In this paper, taking the No. 4 coal seam of Gaojiapu Coal Mine in Shaanxi Province, China, as the research object, the dynamic failure characteristics and mechanism of coal burst under different mining disturbance stress paths are studied by using the self-developed true triaxial coal-rock dynamic characteristic test system. The mechanical properties and dynamic failure characteristics under quasi-static, cyclic, and transient disturbance paths were investigated. The research conclusions can enrich our understanding of the triggering mechanism of coal bursts in real deep engineering.

## 2. Experimental Setup and Procedure

### 2.1. Equipment Setup

The true triaxial coal-rock dynamic behavior testing system was developed by the research team of rock burst in China University of Mining and Technology (Figure 1). The testing system is designed for conducting static and/or dynamic experiments, including the host unit, oil source, oil cooler machine, electric control cabinet, control system, air gun, hydraulic substation, and supporting accessories (such as hydraulic hose and fixture). The unique double closed-loop control technology is used to apply load to the sample in the X, Y, and Z directions through six independent servo-controlled hydraulic pumps. The X-axis static load loading range is 0–2500 KN, and the Y-axis and Z-axis static load loading range is 0–1500 KN. A forced drop bar is installed on one side of the Y-axis to finish the unloading operation instantly. One side of the X-axis applies a one-dimensional stress wave

through the Hopkinson pressure bar to realize the indoor reproduction of the coal-rock dynamic impact disaster process. A high-precision laser displacement sensor monitored the three-dimensional displacement during the loading process.



**Figure 1.** True triaxial coal-rock dynamic behavior testing system: (a) schematic diagram of equipment; (b) single face unloading part with a droppable loading bar.

## 2.2. Coal Samples

The coal samples were taken from the No. 4 seam of the Gaojiapu Coal Mine in Binchang Mining District, Shaanxi Province, China. All the coal samples were first cut into standard cubes from the coal blocks, which were 75 mm in length, 75 mm in width, and 100 mm in height. Then, the surface of the specimen was smoothed by the grinding machine to ensure that the cross-sectional non-parallelism was  $\nless 0.05$  mm, the diameter deviation of the upper and lower sections was  $\nless 0.3$  mm, and the axial deviation was  $\nless 0.25^\circ$  (Figure 2). A total of 30 cube coal samples are used to investigate the dynamic failure characteristics and triggering mechanism of coal bursts by laboratory testing.



**Figure 2.** Coal samples used in the experiment.

The in-situ stress measurement results obtained by the hollow inclusion method are:  $\sigma_1 = 24$  MPa,  $\sigma_2 = 18$  MPa,  $\sigma_3 = 12$  MPa. Therefore, the ground stress field in the investigated area is dominated by vertical stress, horizontal stress is the minimum principal stress, and the stress level and lateral pressure coefficient are high. The “gob-side entry driving” method was used to improve the recovery rate of coal resources. The width of the section coal pillar between adjacent working faces is about 8 m, and the working surface is susceptible to mining disturbances of the adjacent working surface. The working face has obvious floor heave, top coal caving, and bolt fracture during mining, and the production of the working face is seriously threatened (Figure 3).

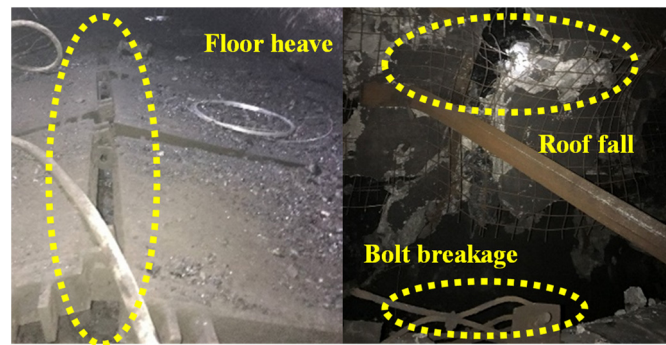


Figure 3. Coal burst characteristics.

2.3. Testing Procedure

As shown in Figure 4, three different forms of mining-induced disturbance load application schemes are designed. The vertical direction is the maximum principal stress used to apply static, cyclic, and transient loads. The horizontal X-axis direction is the intermediate principal stress, while the horizontal Y-axis direction is the minimum principal stress. The unloading is realized through the forced drop bar to simulate the free surface in the mining process.

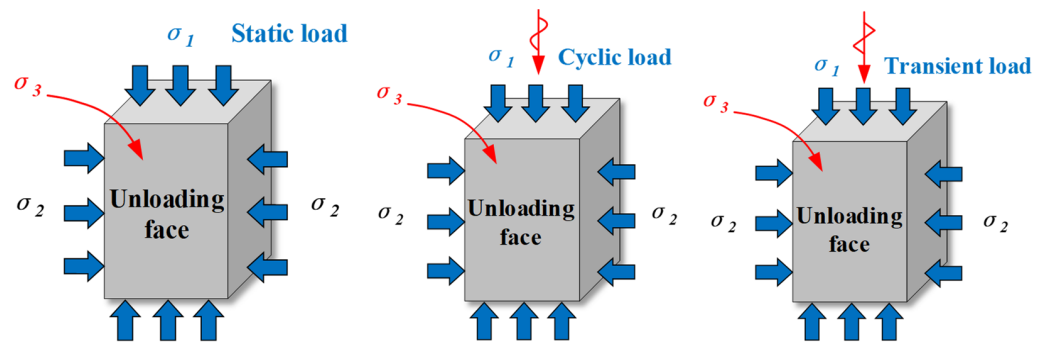


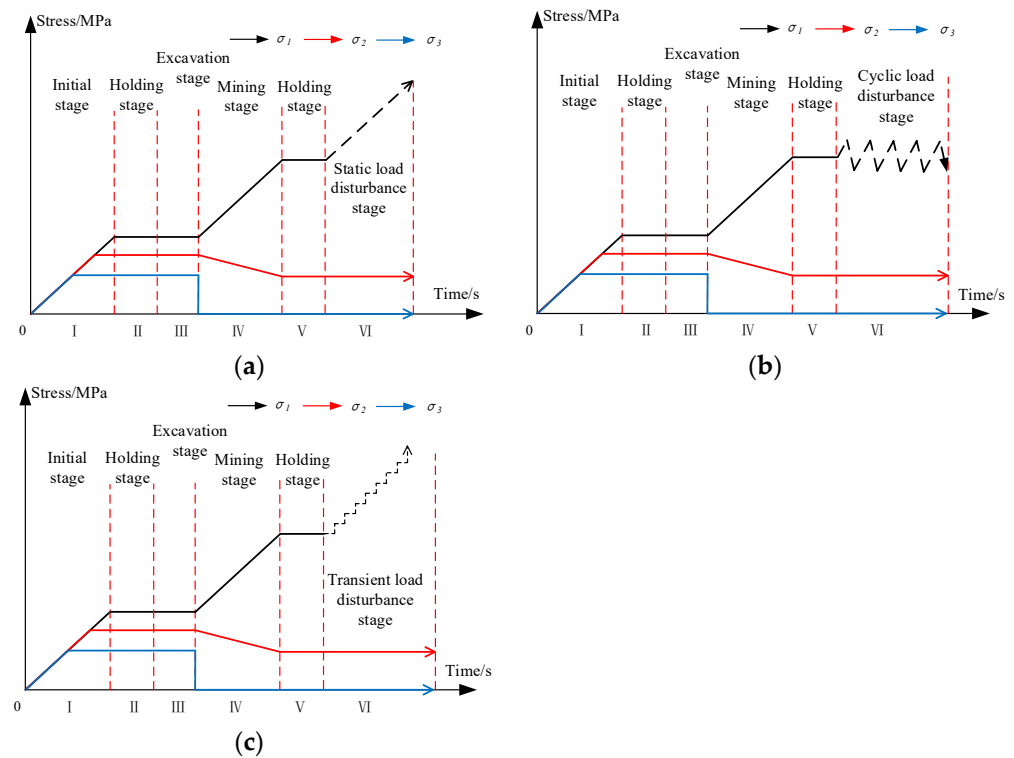
Figure 4. Different types of load disturbance.

Table 1 shows the mining disturbance load experimental scheme with different influence factors. The control variables of static loads include different disturbance stress growth rates: 0.1, 0.2, 0.3, 0.4, 0.5 MPa/s, and different initial stress levels: 10, 12, 14, 16, 18 MPa. The control variables for cyclic loads include different cyclic amplitudes: 2, 4, 6, 8, 10 MPa, and different cyclic frequencies: 0.2, 0.4, 0.6, 0.8, 1 Hz. The control variables for transient loads include different transient increments: 1, 2, 3, 4, 5 MPa, and different initial stress levels: 10, 12, 14, 16, 18 MPa.

Table 1. Different types of coal samples and their numbers.

Load Types	Testing Group	Control Variables	Variables Range
Static load	S-V	Disturbance rate	0.1, 0.2, 0.3, 0.4, 0.5 MPa/s
	S-L	Stress level	10, 12, 14, 16, 18 MPa
Cyclic load	C-A	Cyclic amplitude	2, 4, 6, 8, 10 MPa
	C-F	Cyclic frequency	0.2, 0.4, 0.6, 0.8, 1.0 Hz
Transient load	T-I	Transient increment	1, 2, 3, 4, 5 MPa
	T-L	Stress level	10, 12, 14, 16, 18 MPa

The entire mining stress path under different mining-induced disturbance loads is shown in Figure 5. The disturbance process of each type of load was divided into six stages namely:



**Figure 5.** Stress path of different disturbance stress: (a) static load; (b) cyclic load; (c) transient load.

(1) Initial load stage I: the loads were first increased to the equivalent initial stress environment at a rate of 0.05 MPa/s,  $\sigma_1 = 8$  MPa,  $\sigma_2 = 6$  MPa,  $\sigma_3 = 4$  MPa.

(2) Initial load holding stage II: the loads in the three directions were kept constant for the 30 s.

(3) Roadway excavation stage III: the  $\sigma_3$  direction side is unloaded instantaneously to simulate the actual situation of sudden unloading of stress on one side of the coal body during roadway excavation. While  $\sigma_1$  and  $\sigma_2$  were kept constant for the 30 s.

(4) Working face mining stage IV:  $\sigma_2$  was slowly unloaded to 4 MPa at a disturbance rate of 0.1 MPa/s,  $\sigma_1$  was loaded to different stress levels (10, 12, 14, 16, 18 MPa) at a disturbance rate of 0.2 MPa/s to simulate the actual situation of radial unloading and axial loading during working face mining period.

(5) Load holding stage V: the loads in the three directions were kept constant for the 30 s.

(6) Mining disturbance stage VI:  $\sigma_1$  was loaded at different static load disturbance rates (0.1, 0.2, 0.3, 0.4, 0.5 MPa/s), different cyclic perturbation amplitudes (2, 4, 6, 8, 10 MPa), different cyclic perturbation frequencies (0.2, 0.4, 0.6, 0.8, 1.0 Hz), different transient increments (1, 2, 3, 4, 5 MPa) while  $\sigma_2$  was kept constant until the coal sample is destroyed, and the experiment ends.

### 3. Results

#### 3.1. Relationship between Disturbance Control Variables and Stress Parameters

Figure 6a shows the relationship between different quasi-static stress rates and control variables. When the quasi-static disturbance rate is 0.01 MPa/s, the duration in the disturbance stage is about 142 s, and the peak stress at the final failure is about 26 MPa. As the quasi-static disturbance rate gradually increases, the disturbance duration decreases, and the peak stress increases in the early period and fluctuates later. When the quasi-static disturbance rate is 0.05 MPa/s, the disturbance duration is about 44 s, and the peak stress is about 34 MPa.

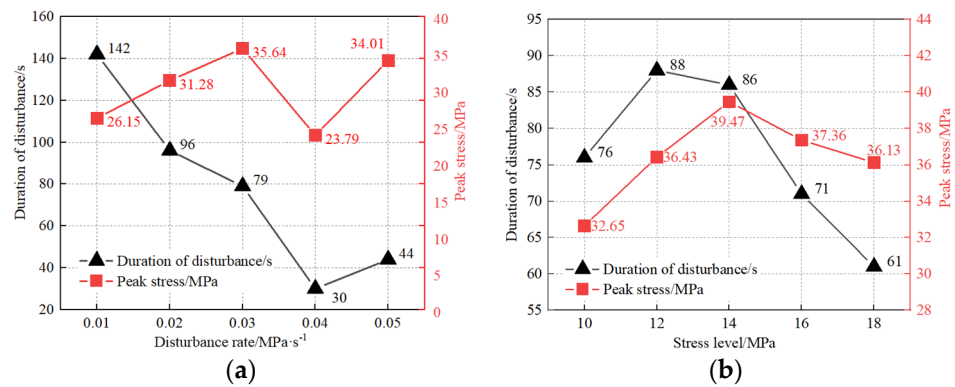


**Figure 6.** Relationship of control variables and quasi-static stress parameters: (a) disturbance rate; (b) stress level.

It shows that at a lower disturbance rate, the development of micro-cracks inside the sample is slower and has enough time to compact, so the sample can last longer disturbance time and finally show more substantial bearing capacity. With the increased disturbance rate, the specimen has been further damaged before the compaction closure, so the duration of the disturbance is gradually reduced. In addition, the correlation between peak stress and perturbation rate is unclear. The reason may be that the number of primary defects in different heterogeneous specimens varies greatly, resulting in peak stress not changing monotonically with changes in perturbation rate.

Figure 6b shows the relationship between different quasi-static stress levels and control variables. When the sample experiences the working face mining period of  $\sigma_1 = 10$  MPa, the corresponding stress concentration factor  $K_r$  is 1.25, the disturbance duration is 76 s, and the stress peak when the specimen is unstable is 32.6 MPa. With the gradual mining of the working face, the disturbance duration and stress peak generally increase first and then decrease. When the stress in the  $\sigma_1$  direction caused by the mining is 14 MPa, the corresponding disturbance duration is 86 s, and the stress peak is 39.5 MPa. As the corresponding stress level before the disturbance gradually increases, the more internal cracks in the specimen and the bearing strength continue to decline. It shows that when the coal-rock mass is high stress, it is straightforward to cause impact damage.

Figure 7a shows the relationship between different cyclic disturbance amplitudes and control variables. When the cyclic amplitude is 2 MPa, the disturbance duration is 3388 s, and the peak stress is 45.66 MPa. When the cyclic amplitude increases to 4 MPa, the disturbance duration decreases to 562 s, and the peak stress decreases sharply to 19.69 MPa. Subsequently, with the increase in cyclic amplitude, the disturbance duration and stress peak did not change significantly. It shows that the lower cyclic disturbance amplitude has less effect on the bearing capacity of the specimen. The stress amplitude of 4MP a seems to be the critical point of a coal sample subjected to cyclic disturbance loads. Once this value is reached or exceeded, the number of internal cracks in the coal sample will increase by an order of magnitude, and the stress peak and damage of the corresponding sample will reach a relatively stable level, which is no longer affected by the cyclic amplitude.

Figure 7b shows the relationship between different cyclic disturbance frequencies and control variables. When the cycle frequency is 0.2 Hz, the disturbance duration is 1526 s, and the peak stress is 39.74 MPa; when the cyclic frequency increases to 0.4 Hz, the disturbance duration decreases to 692 s, and the peak stress is 33.47 MPa. Subsequently, the disturbance duration and stress peak did not change significantly with the increase in cyclic frequency. It is shown that the lower cycle frequency has a certain effect on the bearing capacity of the sample. With the increase of the cyclic frequency, the damage to the specimen formation increases sharply, and the peak stress and ability to withstand disturbances decrease rapidly. Similarly, when the cyclic frequency increases to a specific value, the sample's peak stress and disturbance duration are no longer affected by the cyclic frequency.

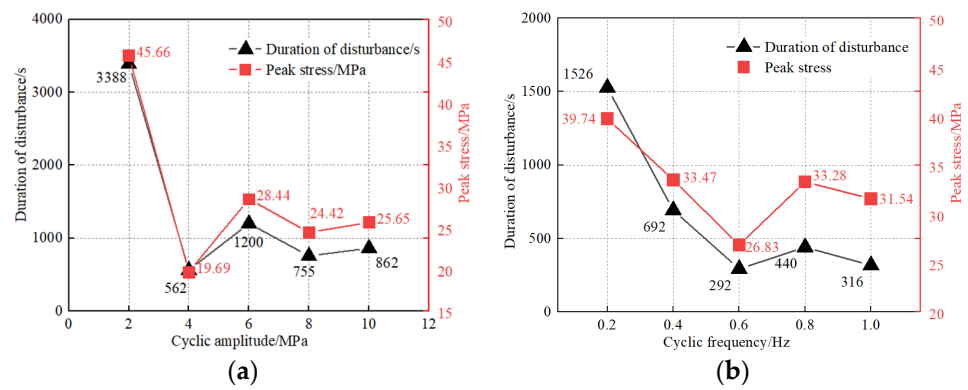


Figure 7. Relationship of control variables and cyclic stress parameters: (a) cyclic amplitude; (b) cyclic frequency.

Figure 8a shows the relationship between different transient disturbance stress increments and control variables. It can be seen that when the transient increment is 1 MPa, the disturbance duration is 121 s, and the peak stress is 25.53 MPa. Then, with the increase of transient increment, the duration of disturbance decreases gradually, while the change rule of stress peak is not apparent. It shows that when the transient increment is low, the damage caused by the sample is less, and the bearing capacity of the mining disturbance load is more vital. After the transient load is enhanced, the damage of the sample increases, and the bearing capacity of the mining disturbance load is significantly reduced.

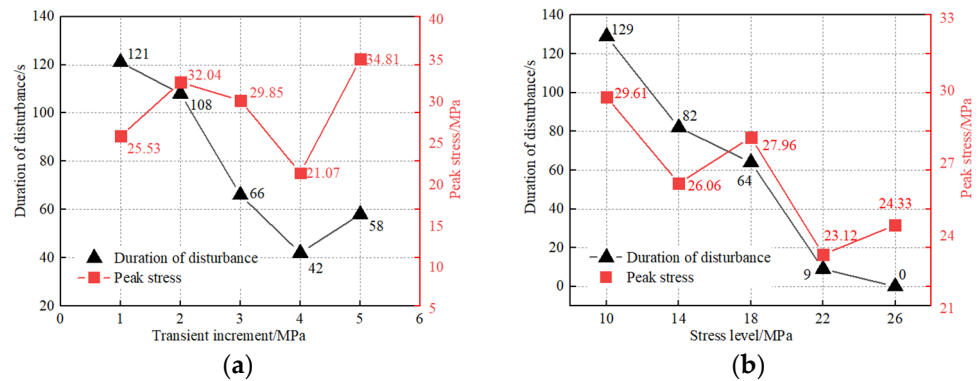


Figure 8. Relationship of control variables and transient stress parameters: (a) transient increment; (b) stress level.

Figure 8b shows the relationship between different transient disturbance stress levels and control variables. It can be seen that when the transient stress level is 10 MPa, the disturbance duration is 129 s, and the peak stress is 29.61 MPa. Subsequently, the perturbation duration and stress peak decrease as the transient level increases.

### 3.2. Relationship between Disturbance Control Variables and Peak Strain

Figures 9–11 show the relationship between different mining-induced disturbance stress and peak strain. The correlation between the mining static load disturbance rate and the peak strain is not apparent, and with the increase in the disturbance rate, the peak stress shows a changing trend of “first lowering—then rising—then decreasing”. However, the disturbance stress level correlates well with the peak strain. As the disturbance stress level increases, the peak strain increases monotonously. It shows that the peak strain of the coal sample under static load disturbance is closely related to the stress level before the disturbance. The higher the stress level, the higher the damage after the impact and the higher the corresponding coal explosion hazard (See Figure 9).

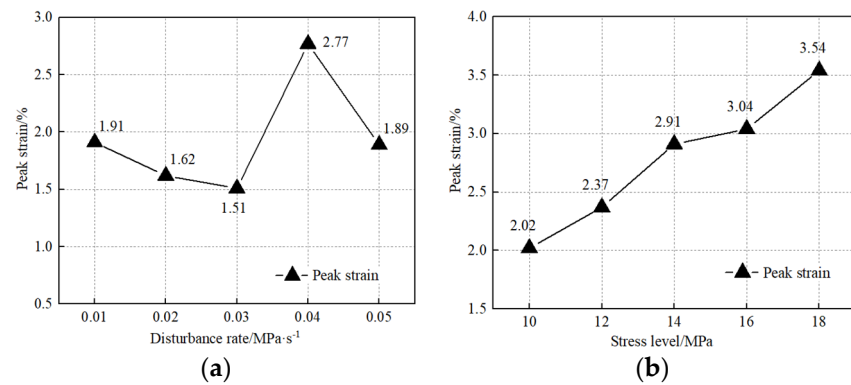


Figure 9. Relationship of static stress control variables and peak strain: (a) disturbance rate; (b) stress level.

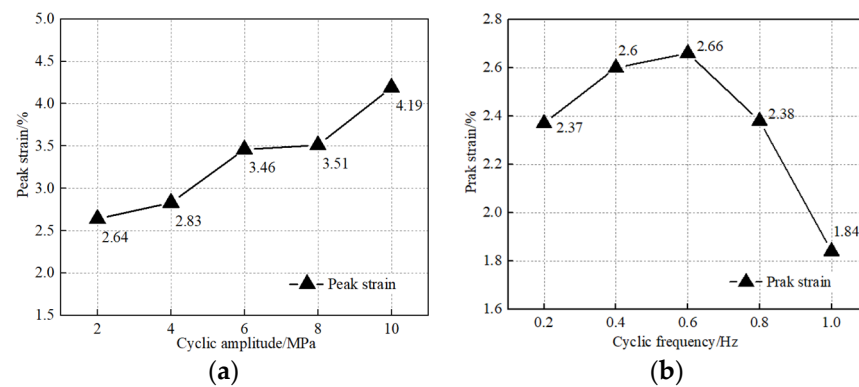


Figure 10. Relationship of cyclic stress control variables and peak strain: (a) cyclic amplitude; (b) cyclic frequency.

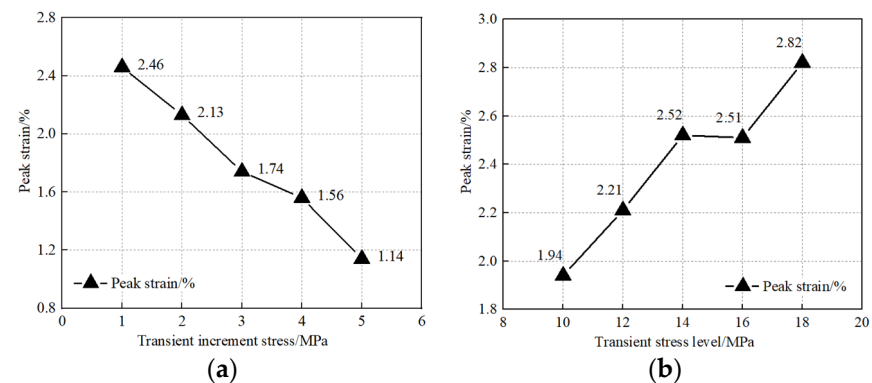


Figure 11. Relationship of transient stress control variables and peak strain: (a) transient increment; (b) stress level.

Figure 10 shows that the coal sample’s peak strain gradually increases with the cyclic amplitude. With the increase of cyclic frequency, the peak strain of coal samples shows a trend of “ first increase-then decrease”. It shows that cyclic amplitude plays a vital role in the crack propagation of coal samples. High cyclic amplitude leads to the generation and development of more internal cracks, increasing peak strain at failure. Under the action of low cycle frequency, it is beneficial to crack propagation inside the sample. When the cyclic frequency is 0.6 Hz, the peak strain is 2.66. When the cycle frequency reaches 1.0 Hz, the peak strain is only 1.84. It is shown that the higher cyclic frequency limits the degree of fracture development in the sample, which causes the micro-fractures to open, close, and expand in the micro-scale. The stress–strain relationship gradually reaches the stable limit state in the macro-scale and is dynamically adjusted to the secondary stability through local instability.

As shown in Figure 11, under the action of transient disturbance, the peak strain decreases linearly with the increase of transient increment. When the transient increment is 1 MPa, the peak strain is about 2.46. When the transient increment is 5 MPa, the peak strain is only 1.14. It indicates that the specimen can withstand more times lower transient incremental perturbations, resulting in more axial strains. The higher transient disturbance increment causes more significant instantaneous damage to the sample. Therefore, when the thick and hard roof is broken, due to the more incredible kinetic energy released instantaneously, the precursory characteristics of roadway deformation before the accident may not be apparent, so it is more difficult to carry out accurate advance predictions.

Contrary to the transient increment, the stress level under the action of mining transient load disturbance is positively correlated with the peak strain at impact failure. When the transient level is 10 MPa, the peak strain is 1.94. When the transient level is 18 MPa, the peak strain is 2.82. This law is consistent with the peak strain law under different quasi-static load levels.

### 3.3. Relationship between Different Disturbance Stress and Failure Characteristics

Figure 12a–c is the relationship between different types of disturbance stress and the dynamic failure characteristics of the samples, and each group of specimens shows a typical pregnancy-trigger-dynamic coal burst generation process. As shown in Figure 12a, after the initial load stage, initial load holding stage, and roadway excavation stage, the integrity of the single-face unloaded sample is good, and no prominent failure characteristics. Then, it enters the mining stage. With radial unloading and axial loading, small particles and block ejection appear at the shoulder angle of the free face. When the load increases to 12 MPa, a small amount of debris is ejected from the middle of the free surface. After entering the static disturbance stage, the crack expands to form a split coal plate. After reaching the limit bearing capacity, a large amount of pulverized coal is sprayed out, and finally, a “V” shaped coal burst pit is formed.

As shown in Figure 12b, at the beginning of the cyclic perturbation, fragment ejection occurs at the top of the free plane, followed by a significant flake crack on the surface. The lower flakes peel off naturally when the disturbance stress level gradually increases. The internal damage develops gradually, and the broken block is pushed out as a whole, eventually forming a significant “dome-like” coal burst pit.

As shown in Figure 12c, unlike the quasi-static and cyclic disturbance loads, the dynamic failure phenomenon is more straightforward before the transient disturbance begins. When the transient load increment is 5 MPa, the free surface of the coal sample suddenly bursts locally, followed by sheet peeling on the sample’s surface, and the free surface damage develops gradually. When the transient load reaches the ultimate bearing strength of the specimen, the specimen suddenly erupts violently and eventually forms a “shallow pit type” coal burst pit.

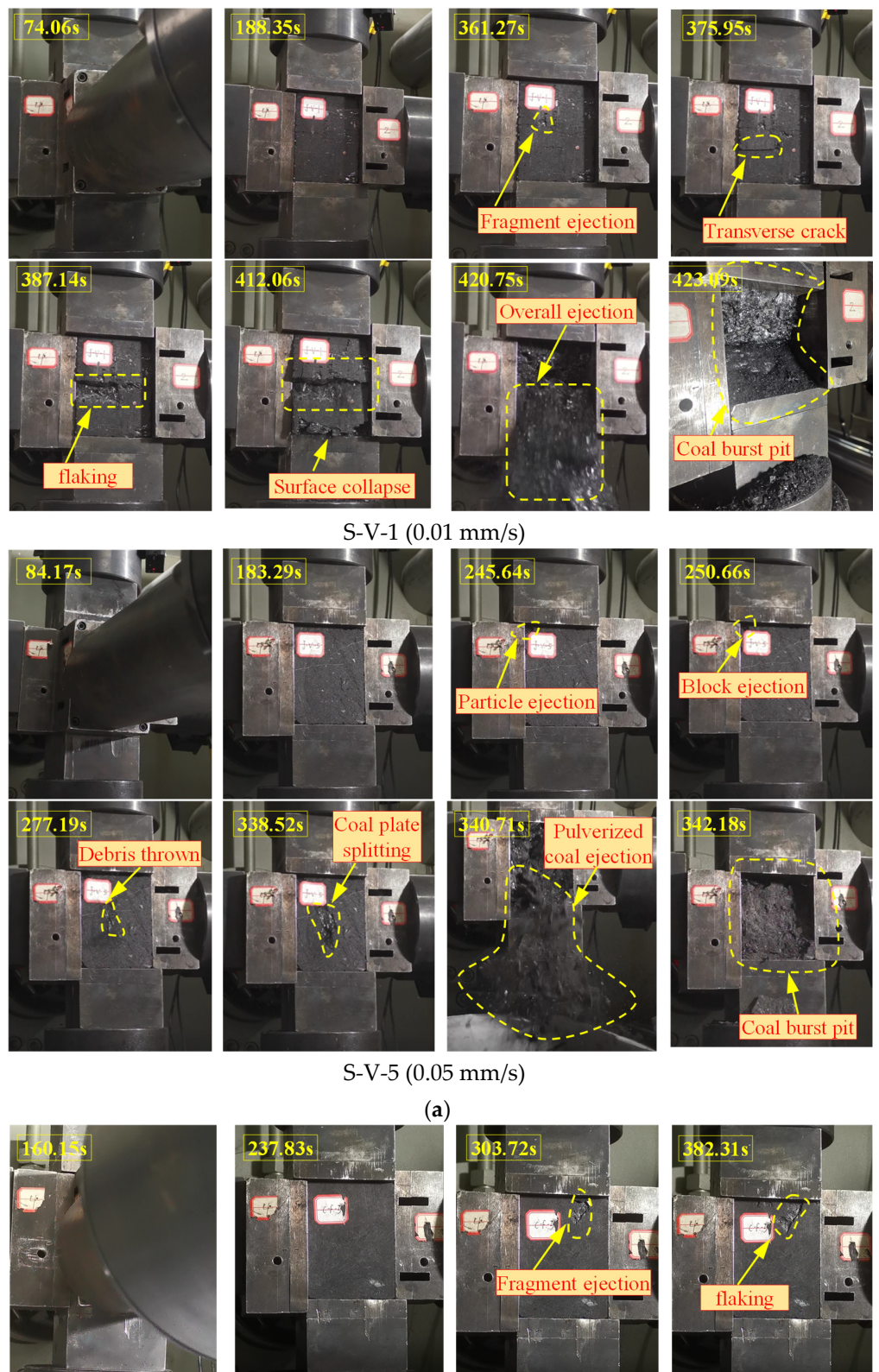


Figure 12. Cont.

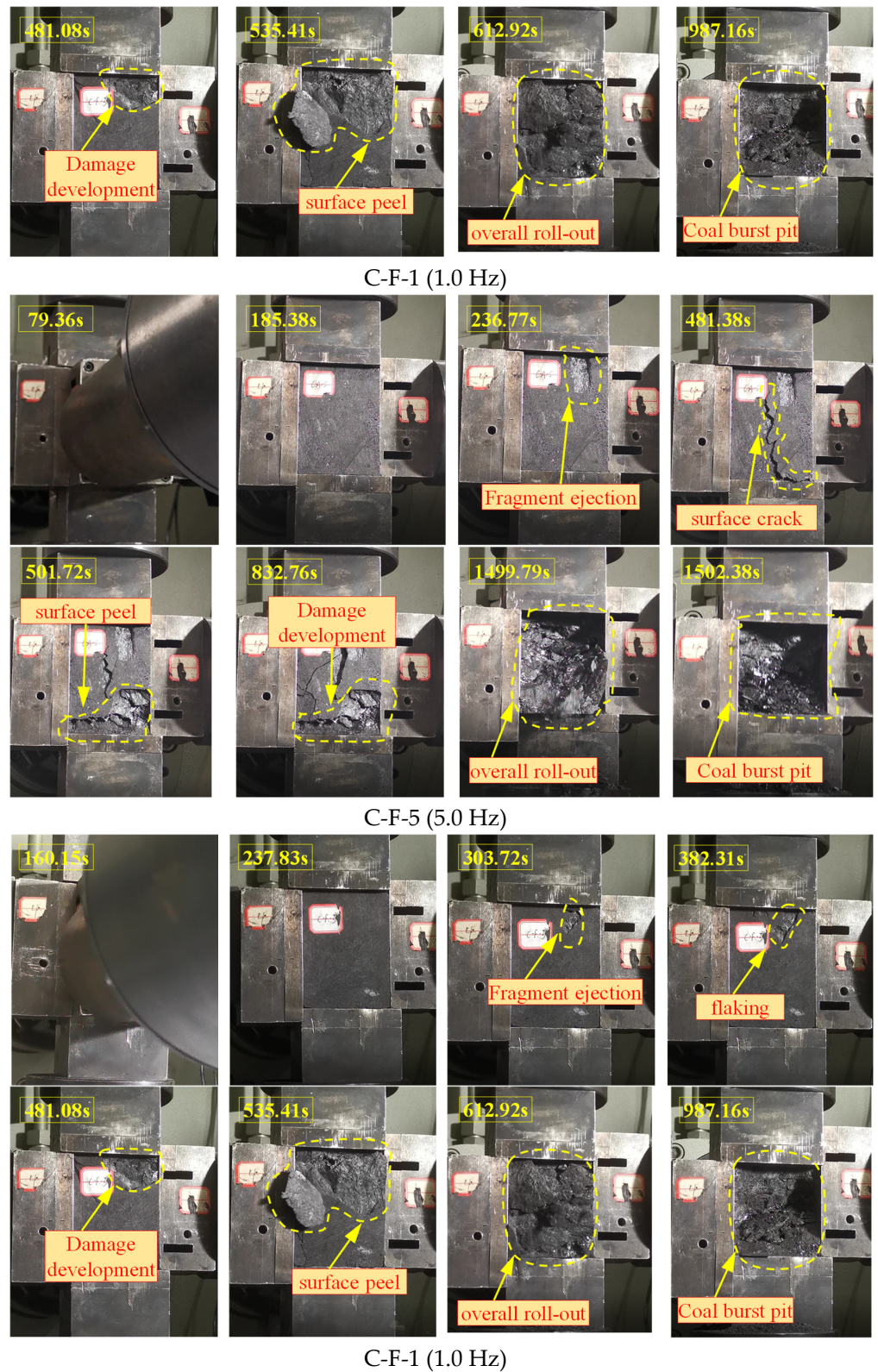
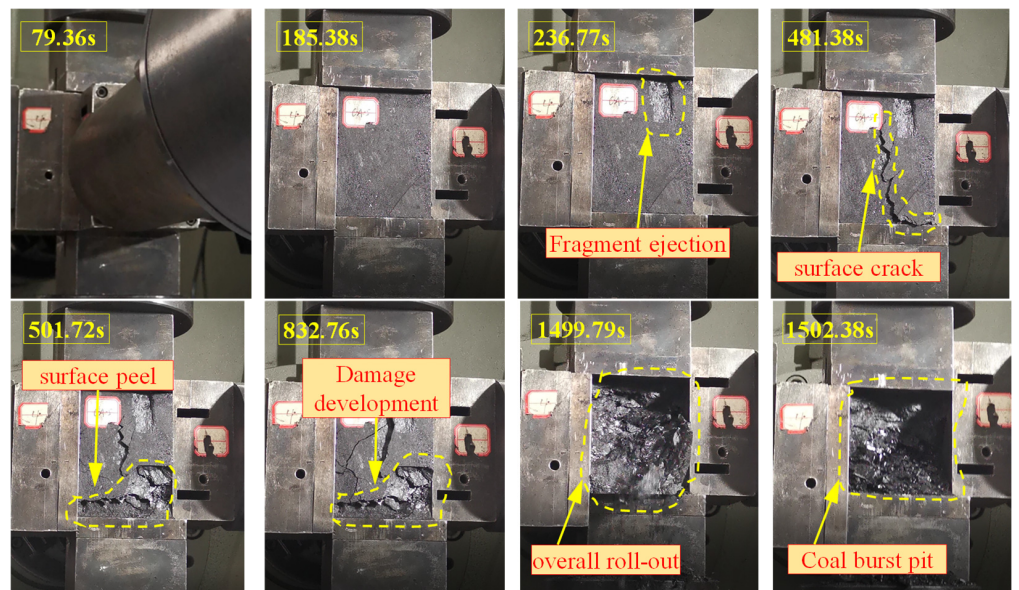
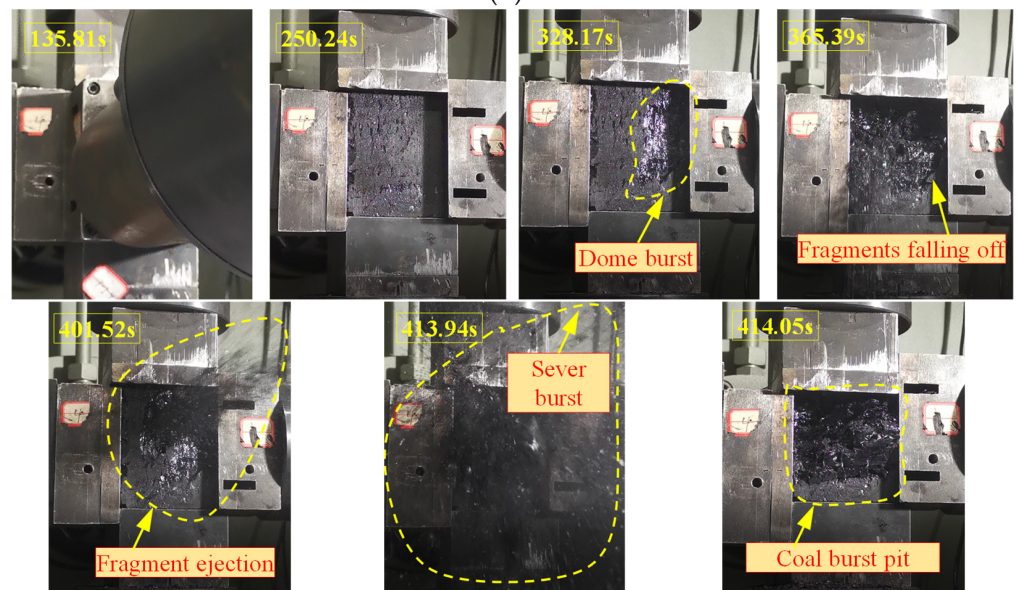


Figure 12. Cont.



C-F-5 (5.0 Hz)

(b)



T-I-1 (1.0 MPa)

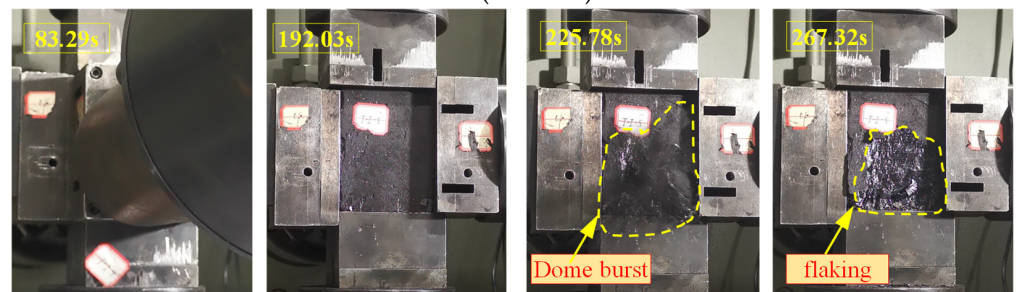


Figure 12. Cont.

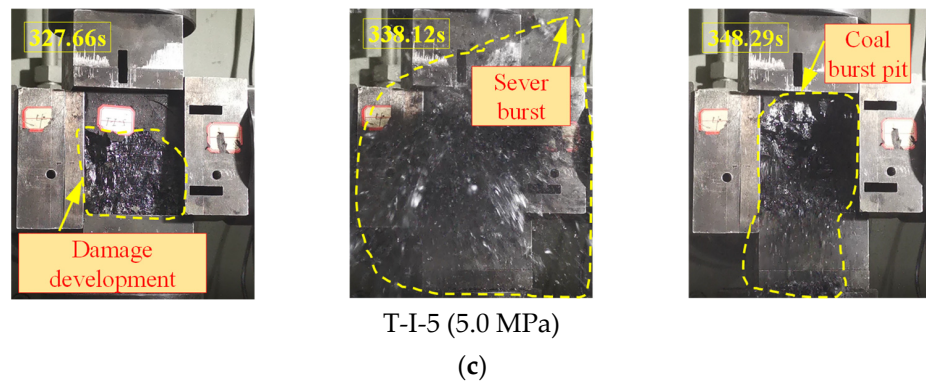


Figure 12. Typical impact failure characteristics of different mining disturbances: (a) static load; (b) cyclic load; (c) transient load.

#### 4. Discussion

##### 4.1. Characteristics of Coal Burst Pits

In exploring the mechanism of rock bursting, the study of rock burst craters is the focus of many scholars. The broad research conclusions obtained by engineering practice [22], indoor test [23], and numerical simulation [24] show that ejection failure is a significant feature of rock bursts. Shallow pit types, deep pit types, and bottomless pit types will be formed after the V-shaped rock burst pit [25]. Different from rock bursts, the occurrence of coal bursts is significantly controlled by mining stress. It is significant to explore the formation characteristics of coal burst pits with different mining disturbance stresses to reveal the mechanism of coal bursts.

Figure 13 shows the evolution laws of coal burst pits under different mining disturbances. As shown in Figure 13a, the quasi-static load is relatively stable, resulting in more cracks inside the sample, which consumes a lot of strain energy. The massive internal fragments are mainly caused by shear failure, manifested as the macroscopic phenomenon of shear into massive fragments. When the coal burst reaches the ultimate load, the residual energy is converted into the kinetic energy of the ejection fragment and promotes it to eject outward. The corresponding rock burst pit depth is the largest, and the debris is the most.

Figure 13b shows that the early free surface is subjected to compressive tension under cyclic loading, showing a macroscopic splitting phenomenon. Subsequently, it was followed by a coal plate shear-buckling fracture. The internal longitudinal cracks are mainly distributed near the free surface. The depth of the coal crater dominated by slab failure is shallow, and the degree of ejection is relatively light. As shown in Figure 13c, the early crack generation and fragment ejection under transient load is not apparent, but the rate of energy accumulation is speedy. Therefore, the fragment ejection dominated by residual energy is the most intense, and the depth of the coal burst pit is relatively shallow.

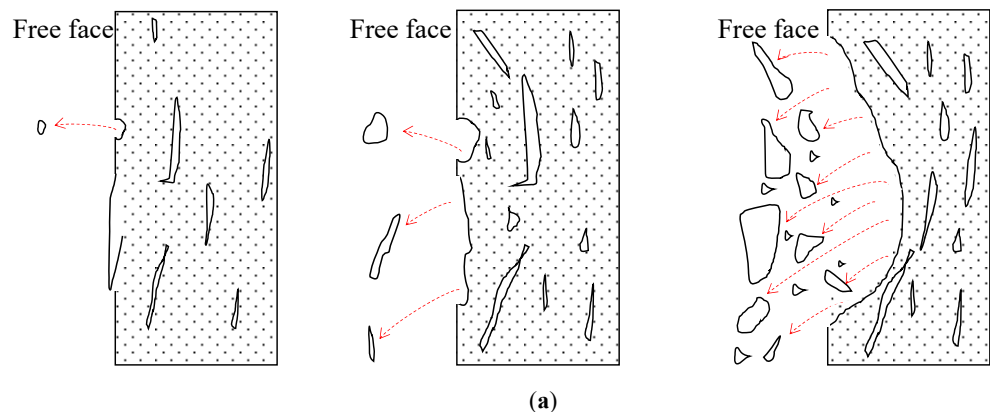
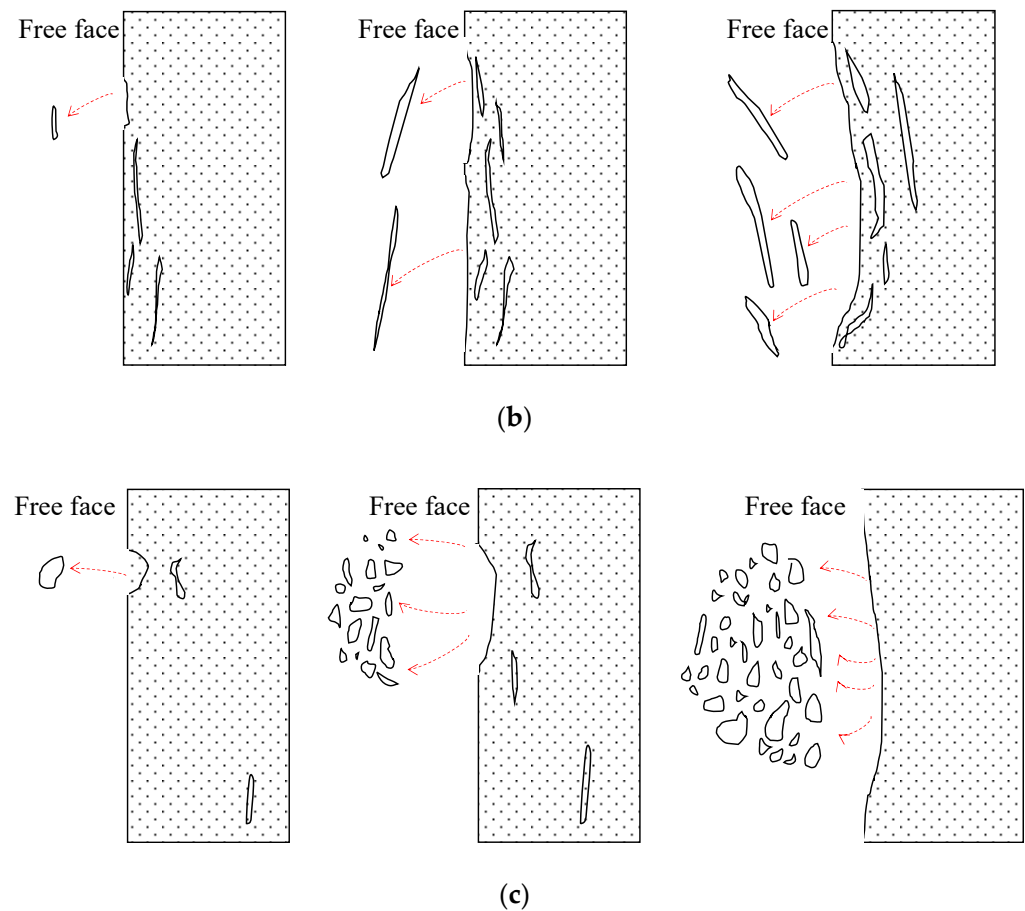


Figure 13. Cont.



**Figure 13.** Characteristics of coal burst pit: (a) static load; (b) cyclic load; (c) transient load.

#### 4.2. Triggering Mechanism of coal Burst under Different Mining-Induced Stress Disturbed

Many researchers pointed that the triggering mechanism of coal burst are different under quasi-static loading, cyclic loading and transient loading. Figure 14 shows the schematic diagram of the coal burst mechanism under different mining disturbances. The mechanical bearing system comprises a roof, a floor surrounding rock, and a coal body. The left side is the bearing stress–strain curve of the surrounding rock, and the right side is the bearing stress–strain curve of coal in front of the working face. Its stiffness and strength are much smaller than that of surrounding rock. In this figure, coal was assumed as a softened material with non-linear behavior, and the roof and floor were abstracted as the whole surrounding rock [26].

It can be seen that the mechanical interpretation of the whole process of coal burst evolution (gestation-trigger-appearance-end) under different mining disturbances is:

(1) A series of classical theories of coal burst have been summarized based on laboratory experiment and field research, including rock strength [27], rigidity [28], energy accumulation and dissipation [29], burst liability [30], and stability [31]. The above burst theories can basically be classified as the research category of static load. When the strain rate caused by the addition and unloading of the mechanical load-bearing system is less than  $10^{-5} \text{ s}^{-1}$ , the process is a quasi-static process. In deep mining, the stress level of the roadway is very high, resulting in the concentration of the surrounding static load stress caused by the excavation of the roadway, and the stress level is close to or even exceeds the critical stress, resulting in the impact damage of the coal body. This type of coal burst is called the high static load dominant type.

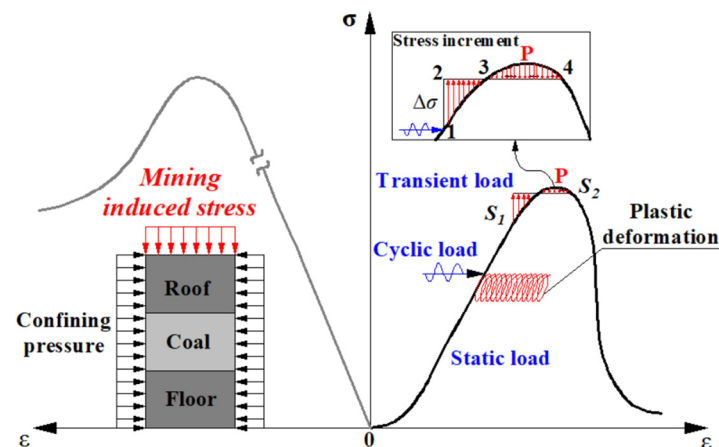


**Figure 14.** Triggering mechanism of coal burst under different disturbing mining-induced stress.

(2) With the great progress of research coal burst theory, such as shearer cutting, cyclic hydro-fracturing, blasting, drilling and seismic waves from adjacent coal burst events, have been proven as a very critical external factor to trigger coal burst [32]. The cyclic loading can well reproduce the periodic loading, which corresponds to the complex and repeated excavation stages during mining operations and underground constructions [33,34]. When the strain rate caused by the addition and unloading of the mechanical load-bearing system is between  $10^{-5} \text{ s}^{-1}$  and  $10^{-4} \text{ s}^{-1}$ , the process is a cyclic disturbance. Such as mine earthquake, especially the far field source, its mode of action is equivalent to cyclic loading and unloading. Due to the heterogeneity of coal and rock materials, each loading and unloading caused by mine vibration load will cause permanent deformation of the coal body. When the action time of dynamic load is long enough, the burst condition similar to the stress state at point  $S_2$  under quasi-static load can be started for the coal body at point  $S_1$  under superimposed dynamic load. Therefore, the dynamic load-induced effect of the dynamic and static load superposition-induced coal burst is called the seismic fatigue load dominant type.

(3) When the strain rate caused by the loading and unloading of the mechanical bearing system is greater than  $10^{-4} \text{ s}^{-1}$ , the inertial force and related dynamic response cannot be ignored. Under the action of transient loads, such as the instantaneous dynamic load caused by fault slip and roof fracture near the working face, its action mode is equivalent to applying an instantaneous stress increment  $\Delta\sigma$ . When the area  $S_{123} > S_{3P4}$ , for the stress state of the coal body at 1 point before the peak, under the action of superimposed dynamic load, the impact condition similar to the stress state at 4 points after the peak under quasi-static load can be started. Therefore, the dynamic load-induced effect of the dynamic and static load superposition-induced coal burst is called the transient load increment dominant type.

## 5. Conclusions

In this paper, the stress–strain relationship and dynamic failure characteristics of coal samples under different mining-induced stress disturbances are systematically studied by using a self-developed true-triaxial coal-rock dynamic characteristic test system. The coal crater’s formation mechanism and the coal burst’s triggering mechanism are discussed. The main conclusions are as follows:

1. Disturbance duration of the coal sample under quasi-static load decreases with the increase of disturbance rate. The peak stress is not affected by the disturbance rate. It increases first and then decreases with the disturbance stress level. The peak strain increases with the increase in stress level. It is beneficial for coal samples to accumulate elastic energy at a relatively stable rate, the corresponding rock burst pit depth is the

largest, and the most debris is formed. It corresponds to a high static load dominant coal burst.

2. Disturbance duration and peak stress of coal samples under cyclic loading decrease with cyclic amplitude and frequency increase. The peak strain increased gradually with the increase of cyclic amplitude. It increased first and then decreased with the increase of peak frequency. The cyclic mining disturbance load is more likely to cause the coal sample to produce flaky or layered damage on the surface of the free surface. The cyclic load leads to the permanent deformation of the coal sample, corresponding to a seismic fatigue load dominant coal burst.
3. The disturbance duration and stress peak of the coal sample under transient load decrease with the increase of transient increment and disturbance stress level. The peak strain decreases linearly with the increase of transient increment and increases with the increase of stress level. The dynamic impact failure characteristics caused by the transient mining disturbance load are superficial. Because the load is generated instantaneously, the energy accumulation and release speed are also speedy. After reaching a certain degree of damage, a violent spray is generated, and the final damage degree is intense. It corresponds to the instantaneous impact dynamic load dominant coal burst.

In conclusion, the mechanism of coal burst is affected by both quasi-static load, cyclic load, and transient load, and the combination of these three can deepen the understanding of the triggering mechanism of coal bursts and provide theoretical guidance for the further plan of monitoring and prevention.

**Author Contributions:** Conceptualization, J.B.; project administration, L.D.; software, X.L.; writing, J.B. and K.W.; investigation, J.C., Y.C. and J.K. All authors have read and agreed to the published version of the manuscript.

**Funding:** This research was carried out with the funded projects: National Natural Science Foundation of China (Grant No. 51874292, 51934007) and National Key Research and Development Program of China (Grant No. 2016YFC0801403). The first author also acknowledges the Postgraduate Research & Practice Innovation Program of Jiangsu Province (KYCX21\_2342).

**Institutional Review Board Statement:** Not applicable.

**Informed Consent Statement:** Not applicable.

**Data Availability Statement:** The authors confirm that the data supporting the findings of this study are available within the article.

**Acknowledgments:** We appreciate the support from the State Key Laboratory of Coal Resources and Safe Mining, and Shaanxi Zhengtong Coal Industry Co., Ltd.

**Conflicts of Interest:** The authors declare that there are no conflict with this publication.

## References

1. Cook, N.G.W. A note on rockbursts considered as a problem of stability. *J. S. Afr. I. Min. Met.* **1965**, *65*, 437–446.
2. Konicek, P.; Ptacek, J.; Waclawik, P.; Kajzar, V. Long-term czech experiences with rockbursts with applicability to today's underground coal mines. *Rock Mech. Rock Eng.* **2019**, *52*, 1447–1458. [[CrossRef](#)]
3. Lu, C.P.; Liu, Y.; Wang, H.Y.; Liu, P.F. Microseismic signals of double-layer hard and thick igneous strata separation and fracturing. *Int. J. Coal Geol.* **2016**, *160*, 28–41. [[CrossRef](#)]
4. Zhang, W.Q.; Mu, C.M.; Xu, D.K.; Li, Z.Q. Energy action mechanism of coal and gas outburst induced by rockburst. *Shock. Vib.* **2021**, *2021*, 5553914. [[CrossRef](#)]
5. Zhang, Y.H.; Ma, J.; Sun, D.Y.; Zhang, L.Y.; Chen, Y.C. AE Characteristics of rockburst tendency for granite influenced by water under uniaxial loading. *Front. Earth Sci.* **2020**, *8*, 55. [[CrossRef](#)]
6. Li, T.; Cai, M.F.; Cai, M. Earthquake-induced unusual gas emission in coalmines—A km-scale in-situ experimental investigation at Laohutai mine. *Int. J. Coal Geol.* **2007**, *71*, 209–224. [[CrossRef](#)]
7. Yang, X.H.; Ren, T.X.; Tan, L.H.; Remennikov, A.; He, X.Q. Developing coal burst propensity index method for Australian coal mines. *Int. J. Min. Sci. Technol.* **2018**, *28*, 783–790. [[CrossRef](#)]

8. Zhang, C.G.; Canbulat, I.; Hebblewhite, B.; Ward, C.R. Assessing coal burst phenomena in mining and insights into directions for future research. *Int. J. Coal Geol.* **2017**, *179*, 28–44. [[CrossRef](#)]
9. Cao, J.R.; Dou, L.M.; Zhu, G.A.; He, J.; Wang, S.C.; Zhou, K.Y. Mechanisms of rock burst in horizontal section mining of a steeply inclined extra-thick coal seam and prevention technology. *Energies* **2020**, *13*, 6043. [[CrossRef](#)]
10. Iannacchione, A.T.; Tadolini, S.C. Occurrence, predication, and control of coal burst events in the US. *Int. J. Min. Sci. Technol.* **2016**, *26*, 39–46. [[CrossRef](#)]
11. Mazaira, A.; Konicek, P. Intense rockburst impacts in deep underground construction and their prevention. *Can. Geotech. J.* **2015**, *52*, 1426–1439. [[CrossRef](#)]
12. Ouyang, Z.H.; Li, C.H.; Xu, W.C.; Li, H.J. Measurements of in situ stress and mining-induced stress in Beiminghe Iron Mine of China. *J. Cent. South Univ.* **2009**, *16*, 85–90. [[CrossRef](#)]
13. Bai, J.Z.; Dou, L.M.; Li, J.Z.; Zhou, K.Y.; Cao, J.R.; Kan, J.L. Mechanism of coal burst triggered by mining-induced fault slip under high-stress conditions: A case study. *Front. Earth Sci.* **2022**, *10*, 884974. [[CrossRef](#)]
14. Li, S.W.; Gao, M.Z.; Yang, X.J.; Zhang, R.; Ren, L.; Zhang, Z.P.; Li, G.; Zhang, Z.T.; Xie, J. Numerical simulation of spatial distributions of mining-induced stress and fracture fields for three coal mining layouts. *J. Rock Mech. Geotech. Eng.* **2018**, *10*, 907–913. [[CrossRef](#)]
15. Zhang, Z.T.; Xie, H.P.; Gao, M.Z.; Xie, J. Mining-induced coal permeability change under different mining layouts. *Rock Mech. Rock Eng.* **2016**, *49*, 3753–3768. [[CrossRef](#)]
16. Zhang, C.; Bai, Q.S.; Chen, Y.H. Using stress path-dependent permeability law to evaluate permeability enhancement and coalbed methane flow in protected coal seam: A case study. *Geomech. Geophys. Geol.* **2020**, *6*, 53–78. [[CrossRef](#)]
17. Guo, Y.B.; Zhou, H.W.; Rong, T.L.; Wang, L.J.; Zhong, J.C.; Ren, W.G.; Chen, J. Disturbance characteristics of deep coal mass under the mining stress path. *J. China Coal Soc.* **2018**, *43*, 3072–3079. [[CrossRef](#)]
18. Xue, Y.; Dang, F.N.; Cao, Z.Z.; Du, F.; Ren, J.; Chang, X.; Gao, F. Deformation, permeability and acoustic emission characteristics of coal masses under mining-induced stress paths. *Energies* **2018**, *11*, 2233. [[CrossRef](#)]
19. Li, X.B.; Cao, W.Z.; Zhou, Z.L.; Zou, Y. Influence of stress path on excavation unloading response. *Tunn. Undergr. Space Technol.* **2014**, *42*, 237–246. [[CrossRef](#)]
20. Xue, D.J.; Wang, J.Q.; Zhao, Y.W.; Zhou, H.W. Quantitative determination of mining-induced discontinuous stress drop in coal. *Int. J. Min. Sci. Technol.* **2018**, *111*, 1–11. [[CrossRef](#)]
21. Bai, J.Z.; Dou, L.M.; Małkowski, P.; Zhou, K.Y.; Chai, Y.J. Mechanical properties and damage behavior of rock-coal-rock combined samples under coupled static and dynamic loads. *Geofluids* **2021**, *2021*, 3181697. [[CrossRef](#)]
22. Li, T.Z.; Li, Y.X.; Yang, X.L. Rock burst prediction based on genetic algorithms and extreme learning machine. *J. Cent. South Univ.* **2017**, *24*, 2105–2113. [[CrossRef](#)]
23. Alexeev, A.; Revva, V.; Alyshev, N.; Zhitlyonok, D.M. True triaxial loading apparatus and its application to coal outburst prediction. *Int. J. Coal. Geol.* **2004**, *58*, 245–250. [[CrossRef](#)]
24. He, M.C.; Miao, J.L.; Feng, J.L. Rock burst process of limestone and its acoustic emission characteristics under true-triaxial unloading conditions. *Int. J. Rock Mech. Min. Sci.* **2009**, *47*, 286–298. [[CrossRef](#)]
25. Jiang, Q.; Feng, X.T.; Xiang, T.B.; Su, G.S. Rockburst characteristics and numerical simulation based on a new energy index: A case study of a tunnel at 2500 m depth. *B Eng. Geol. Environ.* **2010**, *69*, 381–388. [[CrossRef](#)]
26. Cai, W.; Dou, L.M.; Si, G.Y.; Cao, A.Y.; Gong, S.Y.; Wang, G.F.; Yuan, S.S. A new seismic-based strain energy methodology for coal burst forecasting in underground coal mines. *Int. J. Rock Mech. Min. Sci.* **2019**, *123*, 104086. [[CrossRef](#)]
27. Bräuner, G. *Rockbursts in Coal Mines and Their Prevention*; CRC Press: Boca Raton, FL, USA, 1994.
28. Chen, Z.H.; Tang, C.A.; Huang, R.Q. A double rock sample model for rockbursts. *Int. J. Rock Mech. Min. Sci.* **1997**, *34*, 991–1000. [[CrossRef](#)]
29. Xu, Y.H.; Cai, M. Influence of strain energy released from a test machine on rock failure process. *Can. Geotech. J.* **2017**, *55*, 777–791. [[CrossRef](#)]
30. Cai, W.; Dou, L.M.; Si, G.Y.; Cao, A.Y.; He, J.; Liu, S. A principal component analysis/fuzzy comprehensive evaluation model for coal burst liability assessment. *Int. J. Rock Mech. Min. Sci.* **2016**, *81*, 62–69. [[CrossRef](#)]
31. Linkov, A.M. Rockbursts and the instability of rock masses. *Int. J. Rock Mech. Min. Sci. Geom. Abstr.* **1996**, *33*, 727–732. [[CrossRef](#)]
32. Zhang, M.; Dou, L.M.; Konietzky, H.; Song, Z.Y.; Huang, S. Cyclic fatigue characteristics of strong burst-prone coal: Experimental insights from energy dissipation, hysteresis and micro-seismicity. *Int. J. Fatigue* **2020**, *133*, 105429. [[CrossRef](#)]
33. Zhu, G.A.; Dou, L.M.; Wang, C.B.; Ding, Z.W.; Feng, Z.J.; Xue, F. Experimental study of rock burst in coal samples under overstress and true-triaxial unloading through passive velocity tomography. *Saf. Sci.* **2019**, *117*, 388–403. [[CrossRef](#)]
34. Bai, J.Z.; Dou, L.M.; Cai, W.; Gong, S.Y.; Shen, W.; Tian, X.Y.; Ma, H.J. An integration method of bursting strain energy and seismic velocity tomography for coal burst hazard assessment. *Lithosphere* **2022**, *2022*, 2070540. [[CrossRef](#)]